Research Article | Vol. 31, No. 26 / 18 Dec 2023 / Optics Express 44283
Optics EXPRESS

Exploring the impact of longitudinal modulation on the twisting angle in Pancharatnam-Berry phase-based waveguides

STREE VITHYA ARUMUGAM,[1] CHANDROTH P. JISHA,[1,4] LORENZO MARRUCCI,[2] ALESSANDRO ALBERUCCI,[1,5] AND STEFAN NOLTE[1,3]

[1]Friedrich Schiller University, Institute of Applied Physics, Albert-Einstein-Str. 15, 07745, Jena, Germany
[2]Dipartimento di Fisica "Ettore Pancini", Università di Napoli Federico II, Complesso Universitario di Monte Sant'Angelo, Via Cintia, 80126 Napoli, Italy
[3]Fraunhofer Institute for Applied Optics and Precision Engineering IOF, Albert-Einstein-Str. 7, 07745, Jena, Germany
[4]jisha.chandroth.pannian@uni-jena.de
[5]alessandro.alberucci@uni-jena.de

Abstract: A circularly polarized (CP) beam propagating in a rotated anisotropic material acquires an additional phase delay proportional to the local rotation angle. This phase delay is a particular kind of geometric phase, the Pancharatnam-Berry phase (PBP), stemming from the path of the beam polarization on the Poincaré sphere. A transverse gradient in the geometric phase can thus be imparted by inhomogeneous rotation of the material, with no transverse gradient in the dynamic phase. A waveguide based upon this principle can be induced when the gradient accumulates in propagation, the latter requiring a longitudinal rotation in the optic axis synchronized with the natural rotation of the light polarization. Here, we evaluate numerically and theoretically the robustness of PBP-based waveguides, in the presence of a mismatch between the birefringence length and the external modulation. We find that the mismatch affects mainly the polarization of the quasi-mode, while the confinement is only slightly perturbed.

1. Introduction

Dielectric optical waveguides confine light in a certain region of space via a gradient in the refractive index - of infinite magnitude in the case of step-index waveguides- capable of tilting inwards all the optical rays included in a given cone, the latter determining the numerical aperture of the waveguide [1]. In wave terms, an exponential decay of the field in the transverse plane needs to be ensured, using total internal reflection as in the previous example, or other optical effects such as stop band-gap in periodic structures [2]. In all of these cases, a transverse modulation of the dynamic phase of the field is required, and it is provided by a transverse gradient of some sort in the refractive index. In 2014 a new way to trap light using a gauge field [3], the gauge field being some kind of synthetic pseudo-magnetic field acting on the photons [4], was theoretically proposed. The core idea is to maintain the local light dispersion (i.e., the refractive index), but to shift it in the transformed domain by some kind of geometrical transformation. Experimental demonstrations were provided in fiber loops [5,6], in the discrete case of waveguide arrays [7], in photonic crystals [8], and in the case of twisted anisotropic material [9,10]. In the last case, the gauge field can be identified with the local rotation of the dielectric tensor, providing an additional phase contribution called the Pancharatnam-Berry Phase (PBP) [10,11]. The PBP is a geometric phase [12–14] originating from the motion of the optical polarization on the Poincaré sphere, as first demonstrated by Pancharatnam [15]. In a longitudinally (i.e., along the propagation direction) homogeneous material, the PBP is periodic: it reaches a maximum equal

#505538 https://doi.org/10.1364/OE.505538
Journal © 2023 Received 8 Sep 2023; revised 3 Nov 2023; accepted 8 Nov 2023; published 13 Dec 2023

Optics EXPRESS

to twice the rotation angle at half-wave plate (HWP) distance [16,17], but then goes back to zero in the following HWP length [10]. The lack of accumulation of PBP allows optical waveguiding only through the Kapitza effect [18]. A much stronger waveguiding can instead be achieved by longitudinally modulating the dielectric tensor along the propagation direction in a perfectly synchronized way with the polarization rotation due to the birefringence [9], with a mechanism similar to quasi-phase matching in nonlinear optics [19]. This process has been experimentally demonstrated in the linear regime with segmented waveguides [9] and in the nonlinear regime with a continuously rotated liquid crystal [20]. An open and fundamental question is how much the optical waveguiding is robust when there is a mismatch between the birefringence length and the external modulation. For continuous wave or narrow bandwidth pulses, the point to assess is how much the confinement depends on the wavelength. Here we address these problems using a mix of theoretical and numerical simulations based upon an FDTD solver. We show how the PBP waveguides are robust to changes in the period, the biggest change being in the transverse profile and in the polarization structure.

2. Theory

2.1. Resonant case

We consider an uniaxial anisotropic material where the refractive indices are $n_\perp$ and $n_\parallel$ for electric fields polarized normal and parallel to the optic axis, respectively. We also define the optical birefringence $\Delta n = n_\parallel - n_\perp$. We introduce the unit vector $\hat{n}$ parallel in each point to the optic axis. The paraxial beams considered here are monochromatic with vacuum wave number $k_0 = 2\pi/\lambda$ and propagate along z. To avoid any gradient in the extraordinary refractive index, the optic axis is taken normal to the propagation direction (thus $\hat{n} \cdot \hat{z} = 0$). The twisting angle θ is the angle between the optic axis and $\hat{y}$, in turn providing $\hat{n} = \cos\theta\hat{y} - \sin\theta\hat{x}$ [see Fig. 1(a) for a graphical definition]. For homogeneous θ and dubbing $\delta = k_0\Delta n z$ the phase retardation, the PBP $\Delta\varphi_{\text{geo}}$ for circular polarizations (CPs) and small enough θ is approximately

$$\Delta\varphi_{\text{geo}}(\delta) \approx \pm 2\theta \sin^2\left(\frac{\delta}{2}\right) \tag{1}$$

with respect to the untwisted case ($\theta = 0$) [18,21]. The $\pm$ sign shows that positive or negative phase delays depend on the handedness of the launched CP. As discussed in the introduction, the PBP periodically vanishes, see the blue dashed line in Fig. 1(b). A net accumulation in propagation requires a switch in the sign of θ at exactly half of each birefringence length, $\Lambda_{\text{bir}} = \lambda/\Delta n$, see the red solid line in Fig. 1. This can be easily understood first remembering that, at $z = \Lambda_{\text{bir}}/2$, the handedness of the CP is inverted; secondly, from Eq. (1) a change in the sign of θ switches which of the CP undergoes a positive or negative phase accumulation. Summarizing, longitudinal modulations of θ synchronized with the natural oscillation of the polarization yield a monotonic behavior for $\Delta\varphi_{\text{geo}}$, in full analogy with QPM (Quasi-Phase Matching) in nonlinear optics.

We are interested in the case of a more generic periodic function $f(z) = f(z + \Lambda_{\text{bir}})$ featuring a vanishing average value, and a maximum and minimum equal to 1 and -1, respectively. The twisting angle can thus be written as $\theta(x, z) = f(z)U(x)$, where the dependence on y is neglected given we are interested in the simplest (1+1)D case. An example of optic axis rotation along x leading to waveguiding is provided in Fig. 1(c). After defining $\overline{n} = (n_\parallel + n_\perp)/2$ as the average refractive index, the propagation of the slow envelope A_{CP} of CP light can be modelled via a scalar Schrödinger equation [9]

$$i\frac{\partial A_{CP}}{\partial z} = -\frac{1}{2\overline{n}k_0}\frac{\partial^2 A_{CP}}{\partial x^2} \pm V(x)A_{CP}, \tag{2}$$

Optics EXPRESS

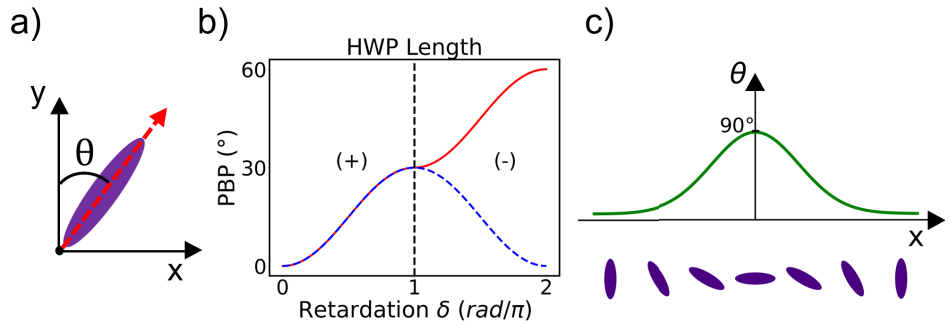

Fig. 1. Sketch of the geometry. (a) Direction of the optic axis -represented by the violet ellipsoid- on the transverse plane xy. (b) Geometric PBP versus the retardation δ in the case of a homogeneous material (blue dashed line) and when the optic axis is rotated at each half-wave plate distance (red solid line). (c) Gaussian distribution along the transverse direction of $\Gamma(x)$, yielding a focusing effect in the case of half-wave plate, and a PBP-based waveguide when the optic axis is periodically rotated along the propagation direction with a period equal to the birefringence length Λ_{bir}.

where we introduced the photonic potential $V(x) = 2\pi f_1 U(x)/\Lambda_{\text{bir}}$ with f_1 being the fundamental harmonic of the periodic function $f(z)$, and where the $\pm$ depends on the handedness of the CP, see Eq. (1). Equation (2) shows how the gradient in the twisting angle behaves like a potential acting on the optical beam, thus capable of guiding the electromagnetic radiation for properly tailored rotations. Equation (2) remains valid only in the case of perfect phase matching, $\Lambda = \Lambda_{\text{bir}}$. Here we are interested in the behavior of light when the latter relation is broken. In the next subsection we will generalize the potential $V(x)$ provided by Eq. (2) by investigating how plane waves propagate in the presence of a longitudinal modulation when the coupling between adjacent transverse positions is neglected.

2.2. Guiding in the presence of phase mismatch

On physical grounds, unidirectional light propagation of the electric field $\boldsymbol{E} = \boldsymbol{A}\exp(ik_0\bar{n}z)$ along z in the paraxial limit can be expressed as the following first-order diffusion problem

$$i\frac{\partial \boldsymbol{A}}{\partial z} = \hat{L}_{\text{diff}}\cdot\boldsymbol{A} + \hat{L}_{\text{inho}}\cdot\boldsymbol{A}, \tag{3}$$

where $\hat{L}_{\text{diff}}$ and $\hat{L}_{\text{inho}}$ account for diffraction and for the point-dependent response of the inhomogeneous material, respectively. Specialized to waveguides, $\hat{L}_{\text{diff}}$ induces the beam broadening due to the spatial dispersion in a homogeneous material. The second operator $\hat{L}_{\text{inho}}$ provides the point-dependent phase modulation capable of counter-acting the beam spreading. In the case of twisted anisotropic materials, in first approximation we have $\hat{L}_{\text{diff}} \approx -(2\bar{n}k_0)^{-1}\partial_x^2$, where $k_0 = 2\pi/\lambda$ is the vacuum wavenumber. The action of the operator $\hat{L}_{\text{inho}}$ can be understood in the plane wave limit, i.e., setting $\hat{L}_{\text{diff}} = 0$. In this limit, we can model the optical propagation using the Jones formalism [22]. By modelling the z-dependent material as a stack of infinitesimally thin layers of anisotropic material encompassing different rotation on the transverse plane xy, the transmission of a slab of thickness z in the circular basis reads

$$\boldsymbol{J}_{total}(z) = e^{i\bar{n}k_0 z}\lim_{N\to\infty}\prod_{m=1}^{N}\exp\left\{-i\frac{k_0\Delta n\,[\hat{s}(\theta_m)\cdot\boldsymbol{\sigma}]}{2}\frac{z}{N}\right\}, \tag{4}$$

where θ_m is the twisting angle in each layer, $\hat{s}(\theta) = \cos(2\theta)\hat{x} - \sin(2\theta)\hat{y}$, $\boldsymbol{\sigma}$ is the Pauli vector and $\Delta n = n_{\parallel} - n_{\perp}$ is the medium birefringence. Thus, $\boldsymbol{A}(z) = \boldsymbol{J}_{total}(z)\cdot\boldsymbol{A}(z=0)$. We are interested in

Optics EXPRESS

a sinusoidal profile of period Λ for the twisting angle θ, $\theta(z) = \theta_M \sin(2\pi z/\Lambda)$. In the adiabatic limit (small $d\theta/dz$ on a wavelength scale), the optical propagation can be normalized defining the phase retardation $\delta = k_0 \Delta n z$. We thus have $\theta(\delta) = \theta_M \sin(\delta/\Gamma)$, where $\Gamma(\lambda) = \Delta n \Lambda/\lambda = \Lambda/\Lambda_{\text{bir}}$. The synchronization parameter Γ determines how much the propagation of plane waves is modified in comparison with the perfectly synchronized case ($\Gamma = 1$), either due to variations on the wavelength λ or on the modulation period Λ.

In the case of waveguiding, the optical field will be periodic along z. The idea is to write down the transmission function of the twisted material by finding numerically the eigenfunctions and eigenvalues of Eq. (4), in turn providing the local polarization and phase delay, respectively. The photonic potential acting in Eq. (2) will then be determined by the transverse distribution of the phase delay, if Λ is much shorter than the Rayleigh distance of the mode. The period of the optical field is not known a priori. Full numerical simulations based upon an FDTD code (see next section) actually show that the period is given by the external modulation, thus Λ, for a wide region around the perfect synchronization case. We will thus consider in our calculation a periodicity of the optical field equal to Λ. Polarization evolution on the Poincaré sphere for one of the eigenmodes family (due to the symmetry, the Stokes parameters of the other family are simply of opposite sign) are shown in Fig. 2(a-c), for different values of Γ and θ_M [23,24]. For small θ_M [Fig. 2(a)] polarization paths are very close to circles featuring S_1 constant. With respect to Γ, the circles move from a small circle nearby $(-1, 0, 0)$ for $\Gamma = 0.5$ to a small circle nearby $(1, 0, 0)$ for $\Gamma = 1.5$, becoming very similar to a meridian for $\Gamma = 1$. S_1 scales almost linearly for intermediate values of Γ. As θ_M gets larger [Fig. 2(b-c)], the polarization paths differs more and more from simple circles, now tracing a full 3D line on the Poincaré sphere. Beyond the full 3D trajectories, the closed path are not exactly centered around $S_2 = 0$, larger the θ_M value the larger the offset is. Remarkably, the slope of the trajectory is almost continuous (S_2 and S_3 are almost perfectly matching, whereas a discrepancy pseudo-periodic with Γ is occurring on S_1) at the end of the loop (transition from blue to red points in the paths), the latter demonstrating that our assumption on the period of the field works well in this range of values.

To provide a more quantitative representation of the results, the behavior of the Stokes parameters versus z in the interval $\Gamma \in [0.4,\ 2]$ is provided in Fig. 2(d-f) for $\theta_M = 15°$ (the same plots for $\theta_M = 5°$ and $\theta_M = 10°$ are provided in the Supplement 1). S_1, which vanishes for $\theta_M = 0$, oscillates with a period $\Lambda_{\text{bir}}/2$. In the region near $\Gamma = 1$, S_2 and S_3 are slightly perturbed with respect to the case $\theta_M = 0$. For Γ larger than 1.5, an additional peak around the center appears: such a peak grows up as Γ increases, until a quasi-sinusoidal profile of period $\Lambda_{\text{bir}}/2$ at $\Gamma = 2$ is achieved. For Γ<1 the period stays constant, but at $\Gamma \approx 0.75$ the oscillations are strongly damped out, yielding an almost uniform distribution along z. On the other side, S_1 follows an almost linear behavior with Γ, with small oscillations superposed to the average value which behave similarly to S_2 and S_3 in terms of periodicity (i.e., doubling of the period for Γ>1, dampening of the oscillations for Γ<1). The overall behavior versus Γ is summarized in Fig. 2(g-i), where we plotted the average Stokes parameters $\overline{S_i} = \int_0^\Lambda S_i(z)dz$ versus the synchronization parameter Γ. In the phase-matched case ($\Gamma = 1$), $\overline{S_2}$ and $\overline{S_3}$ are vanishing, whereas $\overline{S_1}$ takes a small value, directly proportional to θ_M. The condition $\Gamma \neq 1$ affects $\overline{S_1}$ the most, see Fig. 2(d). The slope of $\overline{S_1}$ around $\Gamma = 1$ is very abrupt, with $\overline{S_1}$ changing from -1 to 1. The curve tends to be a step function for $\theta_M \to 0$, whereas it becomes smoother as θ_M increases. For Γ>1.5 a further drop towards zero is observed. In a similar way, the other two Stokes parameters develop a non-null average when $\Gamma \neq 1$. but encompassing more complex and non-monotonic trends. The phase delay plotted in Fig. 2(j), in turn being the quantity which determines the photonic potential and thus the profile of the waveguides, has its maximum located in $\Gamma = 1$, the maximum phase delay being given by $\pi\theta_M$ for small enough θ_M. It is important to stress that in the general case the transverse gradient in the phase delay is given by a mixture of dynamic and geometric phase [25] given that there is no more balance between positive and negative angles, as in the case for $\Gamma = 1$. Summarizing,

Optics EXPRESS

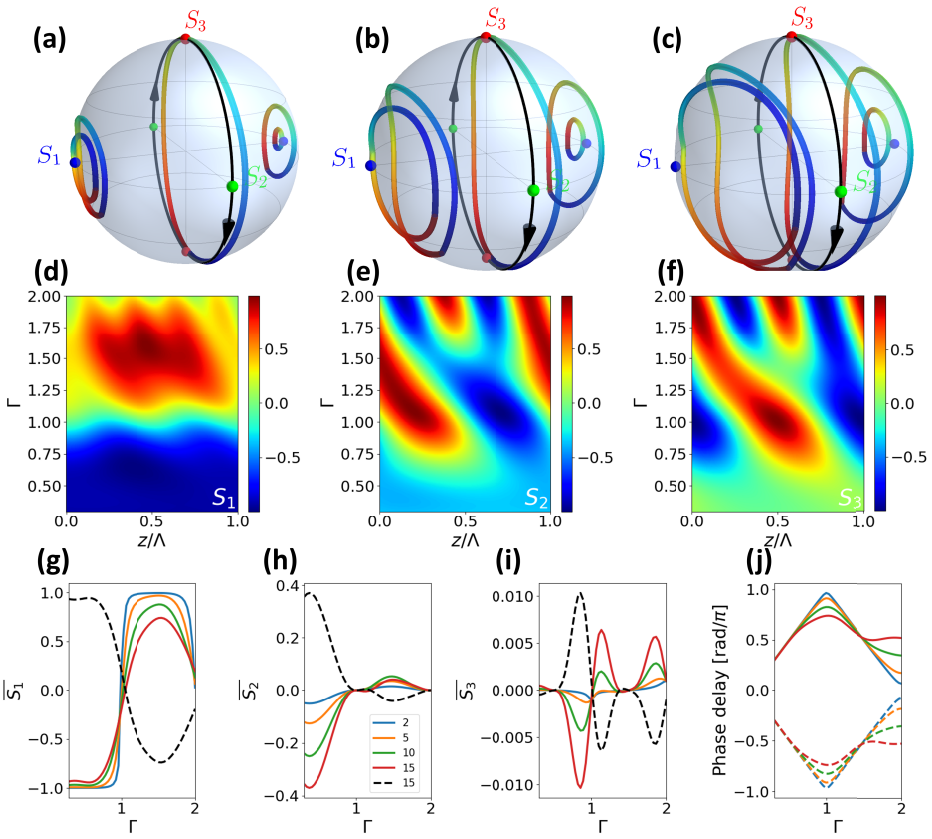

Fig. 2. Plane-wave model considering the optical propagation periodic, with a period Λ fixed by the external modulation. Polarization evolution mapped on the Poincaré sphere for (a) $\theta_M = 5°$, (b) $\theta_M = 10°$, and (c) $\theta_M = 15°$. The five circuits plotted in each sphere correspond to $\Gamma = 0.6,\ 0.8,\ 1,\ 1.2,\ 1.4$, from right to left. The evolution of S_1 (d), S_2 (e) and S_3 (f) for $\theta_M = 15°$ plotted as a heatmap versus the normalized propagation z/Λ (horizontal axis) and the parameter Γ (vertical axis). Averaged Stokes parameters (g-i) and phase delay (j) versus the parameter Γ for one set of eigenfunctions (solid lines). Each curve corresponds to a different angle θ_M, as reported in degrees by the legend in panel (h). The black dashed line in (g-i) corresponds to the values for $\theta_M = 15°$ for the other set of eigenfunctions. The dashed lines in panel (j) is the phase delay perceived by the other set of eigenfunctions.

the plane-wave model provides some insights on how the polarization of the quasi-mode should behave, and how it differs from the cycle RCP-diagonal-LCP-anti-diagonal when the period is no more synchronized with the birefringence length. The most relevant result is that a constant S_1, proportional to $\Gamma - 1$ in an interval near the resonance, should appear in the localized mode. At the next order of relevance, the peaks in the oscillations of S_2 and S_3 should be modified as Γ diverges from 1: for $\Gamma<1$, S_2 and S_3 tends to become uniformly distributed along z; for $\Gamma>1$, a second peak arises, with the profile then continuously evolving towards a halving of the period, achieved when $\Gamma = 2$.

To build a waveguide, we will consider the case where $\lim_{|x|\to\infty} U(x) = 0$, i.e., the cladding of the waveguide is made of untwisted material. To fix the ideas, we set $U(x) = \theta_0 g(x)$, where the maximum of $g(x)$ is equal to 1. Thus, θ_0 is the maximum rotation angle with respect to the cladding regions. We also consider a wavelength λ of 1 μm, and set $n_\perp = 1.5$ and $\Delta n = 0.2$; these parameters are kept unvaried in the remainder of the article. Hereafter we take

Optics EXPRESS

$g(x) = \exp\left(-x^2/w_D^2\right)$ with $w_D = 5\mu$m. The behavior of $V(x)$ versus x and the parameter Γ is plotted in Fig. 3(a) for $\theta_0 = 15°$, where the potential is reported in units of equivalent refractive index changes δn by using the relationship $V \approx -\delta n k_0$. Figure 3(b) shows the corresponding fundamental mode, which is subject to minimal changes for variations in Γ up to ±30%. The white dashed lines delimit the region where a fundamental mode can be calculated using our theoretical approach. Figure 3(c) finally shows the effective index n_{eff} [mode written in the standard form $A_{CP}(x,z) = \psi(x)\exp(ik_0 n_{\text{eff}} z)$] versus the parameter Γ for three different values of the maximum rotation angle θ_0. Thus, the plane-wave predicts quite surprisingly the existence of quasi-modes far away (variations almost up to ±50% in Γ) from the synchronization condition. The size of the fundamental quasi-mode does not even change significantly for variations in Γ of around ±20%, thus showing a seemingly counter-intuitive robustness for the optical confinement. Remarkably, the model employed in this section is a simplification with respect to the actual optical propagation, where diffraction and polarization rotation occurs together. In the next section we thus resort to full numerical simulations of the Maxwell's equations to verify the validity range of the model we developed in this section.

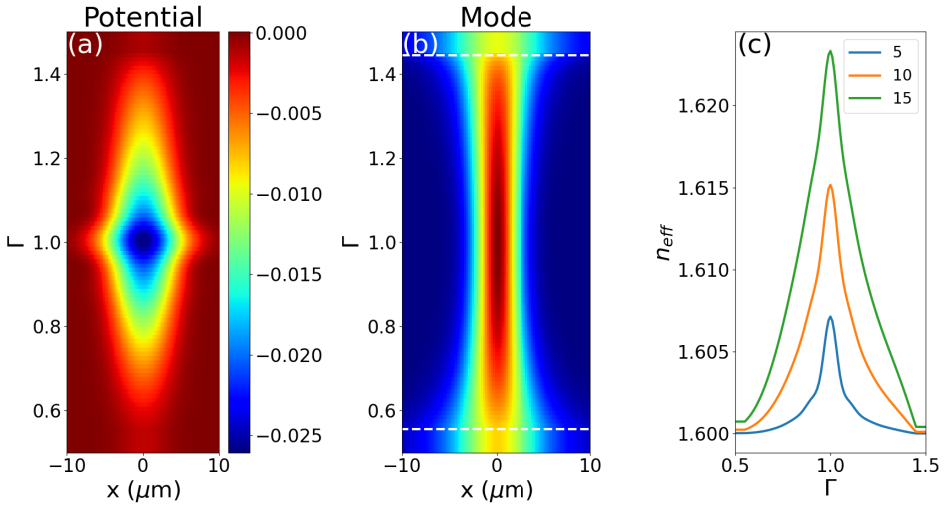

Fig. 3. (a) Photonic potential and (b) the corresponding fundamental mode versus x and phase-matching parameter Γ for $\theta_0 = 15°$. The white dashed lines delimit the range of Γ where the potential is monotonic, thus always supporting at least one guided mode. (c) Effective index n_{eff} of the fundamental mode versus Γ for three different values of θ_0 as indicated in degrees by the legend.

3. FDTD numerical simulations

We performed the parametric study using the open-source software MEEP [26] implementing a finite-difference time-domain (FDTD) algorithm to solve the Maxwell's equations. The (1+1)D approximation permits to perform a parametric investigation versus the period Λ in a reasonable machine time. We started by investigating the propagation of the mode computed from Eq. (2), i.e., a CP mode with a transverse shape dictated by the potential for $\Gamma = 1$ [see Eq. (2)]. Results are plotted in Fig. 4. The period Λ of the longitudinal modulation is varied such that Γ ranges between 0.3 and 5. Additionally, as the waveguiding mechanism is polarization dependent, both circular polarizations are used as input conditions. The RCP quasi-mode is guided without appreciable losses when propagated in a phase-matched PBP waveguide ($\Gamma = 1$). For $0.3<\Gamma<2$, light is confined after an initial radiation loss due to the mode mismatch. The mode mismatch

Optics EXPRESS

includes also the polarization of the beam: Fig. 4(f-j) show that, for Γ away from 1, a significant portion of light is trapped, even when the input is LCP. This is in agreement with Fig. 2(d), where it is shown that for $\Gamma \neq 1$ the average Stokes parameter $\overline{S_1}$ changes as the period moves away from the synchronized case. Surprisingly, the numerical simulations predict that optical confinement takes place over an interval of Γ even more extended than the range predicted by the theoretical description presented in Sec. 2. For short periods, the plane wave model developed above fails due to the kick-in of non-adiabatic effects. In the opposite limit of long periods ($\Gamma \gg 1$), the optical field is no more periodic with Λ, as visible in Fig. 2. For $\Lambda \geq 2\Lambda_{bir}$ (corresponding figures are provided in the Supplement 1) the emergence of a peak around $x = 0$ over the diffracting background demonstrates a weak concentration of light. Some kind of focusing is thus occurring, but the numerical resources (the optical propagation is computed up to $z = 245\ \mu$m) does not allow to establish the existence of a quasi-mode, which nonetheless should be very wide when compared with the transverse size of the numerical grid.

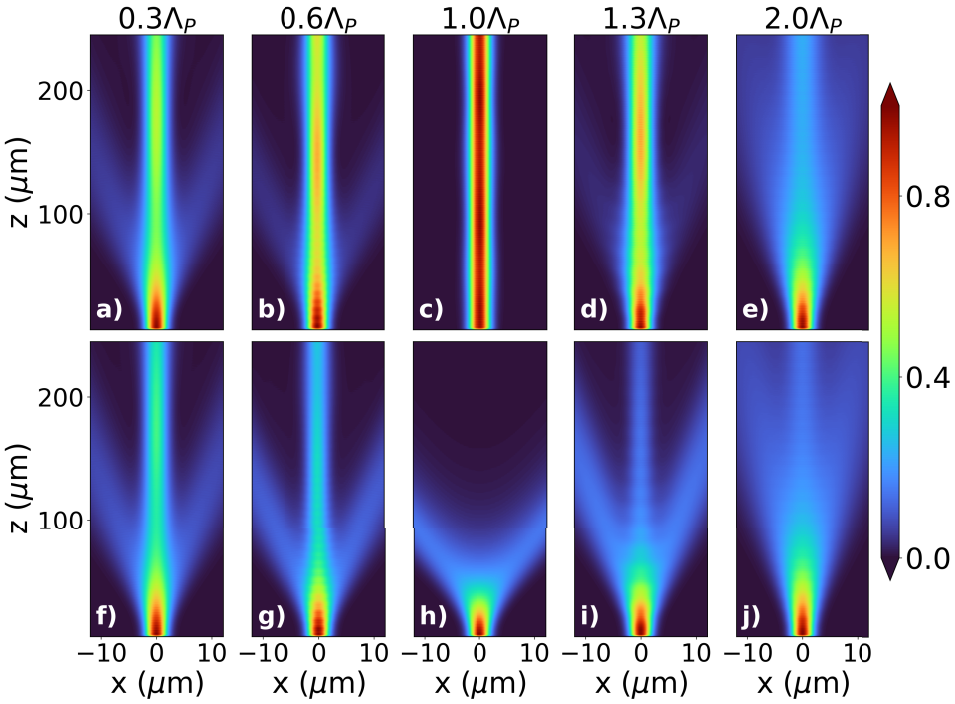

Fig. 4. Intensity distribution of light propagating in a PBP waveguide with $\Delta n = 0.2$, $w_D = 5\ \mu m$ and $\theta_0 = 15°$ when the quasi-mode computed for $\Gamma = 1$ is launched at the input. Each column corresponds to a different period for the longitudinal modulation: Γ is 0.3 (a,f), 0.6 (b,g), 1 (c,h), 1.3 (d,i), 2 (e,j). Top (a-e) and bottom (f-j) rows correspond to RCP and LCP inputs, respectively.

To gain more insights on the waveguide properties, we extract from the numerical simulations the spatial distribution of the Stokes parameters S_1, S_2 and S_3, the latter determining the light polarization in each point. In Fig. 5 the behavior of three Stokes parameters is plotted over a span of 20 μm, taken far enough from the input interface ($z = 200\ \mu$m) to ensure that the stationary regime is achieved. The images of the field in proximity of the interface can be found in the Supplement 1. For $\Gamma = 1$ the polarization periodically flips from RCP to LCP and back to RCP, passing through the diagonal and anti-diagonal states ($|S_2| = 1$) [9,27]. Unlike the ideal case of alternate and longitudinally-homogeneous half-wave plates (i.e., when $f(z)$ is a rectangular

Optics EXPRESS

function), the component S_1 is not vanishing, being in particular subject to a small-amplitude oscillation around a negative value [27], in agreement with the plane wave model (Fig. 2). When $\Gamma \neq 1$, the polarization of the guided waves agrees well with the predictions of Fig. 2(a): S_1 increases linearly with Γ, being at the same time subject to small oscillations with a period comparable with the external modulation. The behavior of S_2 and S_3 is more complicated. First, the periodicity actually depends on the transverse position x: the field in the core region shows a period equal to the external modulation Γ, but on the edges the period is longer, and close to the birefringence length Λ_{bir}. Up to Γ<1.3 the Stokes parameters are almost flat versus x in the core of the waveguide, whereas an appreciable curvature along the transverse direction x is observed for longer modulations, alongside with a strong deformation with respect to the sinusoidal oscillation. In agreement with the plane-wave model [see Fig. 2(e-f)], the FDTD simulations also shows a doubling of the periodicity when $\Gamma = 2$. For Γ approaching 2, the longitudinal profile of the oscillation is quantitatively different from what plotted in Fig. 2(e-f), specifically being smoother along the transverse direction x. As a matter of fact, the longitudinal profile in the plane-wave limit strongly depends on θ_M [see Fig. 2(a-c)], in particular encompassing large deformations -including a longitudinal shift of the peaks- with respect to a pure sinusoidal oscillation. Such a discrepancy can be understood as a consequence of the point-wise interplay between diffraction and the polarization motion on the Poincaré sphere, modelled as a gauge transformation in Ref. [27]. In more detail, the transverse diffusion associated with the diffraction operator tends to smooth out the polarization variations of the quasi-mode in the core region (see Fig. 5 for Γ up to 1.3).

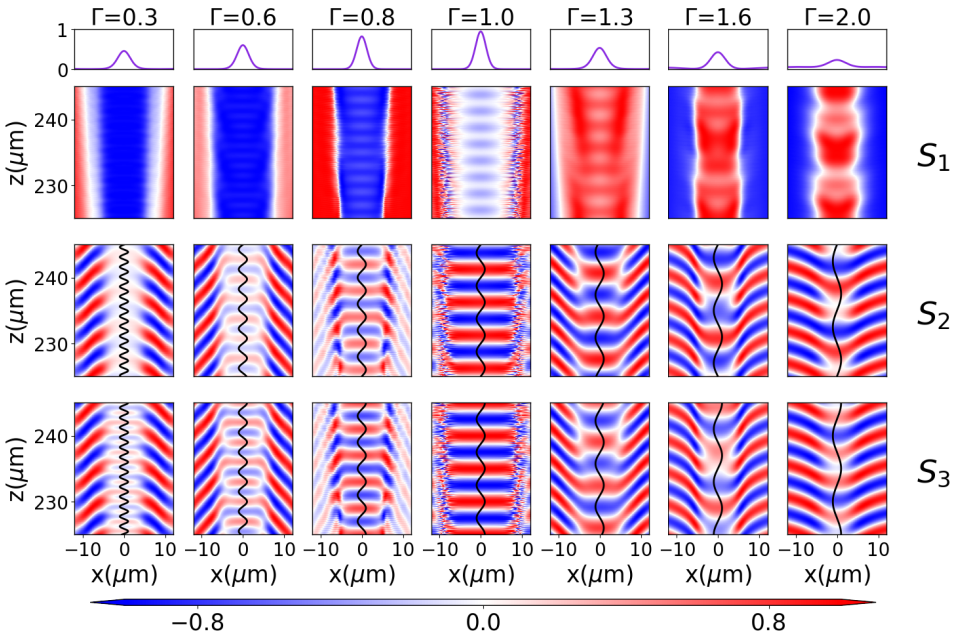

Fig. 5. Cross-section (top row) of the intensity distribution in the stationary regime. Distribution of the Stokes parameters S_1 (second row), S_2 (third row) and S_3 (bottom row) plotted in a portion of the xz plane far enough from the interface to ensure a stationary behavior. Each column corresponds to a different period for the external modulation, i.e., a different Γ, the value being reported at the top. The solid black line shows the longitudinal modulation of the optic axis.

A quantitative comparison between FDTD simulations with a RCP input and the corresponding theoretical results [plotted in Fig. 2(d-j)] is shown in Fig. 6. We compare both the average

Optics EXPRESS

values ($\overline{S}_i$) and the maximum values of the three Stokes parameter once a stationary regime is achieved, see Fig. 6(a). The agreement between the two approaches is quite good for all the three parameters, especially when Γ does not significantly differ from unity. The second comparison is carried out in Fig. 6(b) with respect to the width w of the guided modes (red lines, defined as $2\sqrt{\int I(x)x^2dx/\int I(x)dx}$; $I(x)$ is the intensity distribution) and the amount of guided power in the twisted region (blue lines, integral of the intensity in the interval $[-10,\ 10]\mu$m). The variations versus Γ of the quasi-mode size computed via the FDTD code (input unvaried with Γ and given by the mode for $\Gamma = 1$) and the theoretical results stemming from Fig. 3(b) are in good agreement for $0.8 \leq \Gamma \leq 1.5$. For the same input field, the coupled power is sharply peaked around the condition $\Gamma = 1$ itself, reaching a value of around 70% at the borders of the region where theory ensures the existence of at least one guided mode.

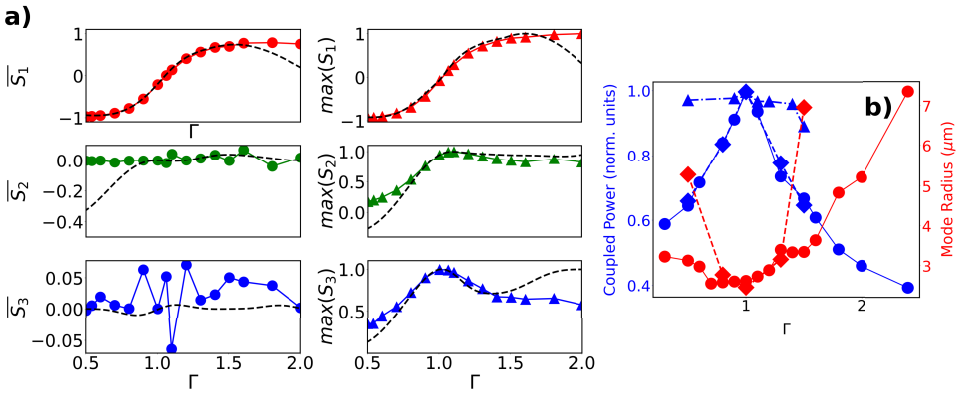

Fig. 6. (a) Comparison of the Stokes parameters S_1 (top row), S_2 (middle row) and S_3 (bottom row) between theory (black dashed line) and FDTD simulations (connected colored circles and triangles) versus Γ when the input is RCP. Left and right column correspond to the average and the maximum value computed over the interval $z \in [200,\ 240]\mu$m in the mid section $x = 0$. (b) Ratio of the guided power (left axis, blue color) and beam radius (right axis, red color) versus Γ. Blue and red solid lines with circles are the coupling efficiency to the waveguide core and the field radius at the output when the input mode is circularly polarized with intensity profile calculated in the case $\Gamma = 1$. Blue dashed line with diamonds is the coupling efficiency computed via the FDTD when the mode is given by the data plotted in Fig. 3(b) but circular polarization. The dashed line with red diamonds is the mode width calculated directly from Fig. 3(b). The blue dash-dotted line with triangles is finally the coupling efficiency derived from FDTD simulations when also the polarization is varied according to the theoretical results plotted in Fig. 2(d-i).

In a second step we computed the guided power once a Gaussian beam of width identical to the theoretical predictions from Fig. 3(b) is launched into the structured material, but keeping the input polarization right circular. The main results for this excitation are depicted by the blue line with diamonds in Fig. 6(b). The coupling efficiency is almost unvaried: the waveguide at $\Gamma = 1$ is strongly guiding (up to 5 modes), and variations in the input beam width yields larger breathing period, but this does not affect significantly the coupled power (see Supplement 1). This behavior agrees with the strong spin-orbit interaction responsible for the optical confinement in twisted anisotropic materials: the correct polarization and the correct intensity profiles need to be launched at the entrance facet of the waveguide to achieve the best coupling efficiency.

To further test the spin-orbit nature of the light guiding, we finally simulated the optical propagation when the input is matched with the theory both in intensity profile (noteworthy, we are slightly simplifying the problem by taking a Gaussian profile of width equal to the theoretical

Optics EXPRESS

mode) and in polarization. We set the input polarization to be equal to the output one that is obtained directly from the FDTD simulations plotted in Fig. 4. The aim is to test the amount of diffraction losses for the quasi-modes emerging from the numerical simulations; indeed, from Fig. 4 we evince that light undergoes trapping -i.e., a negligible amount of diffraction losses per unit length- after a certain distance, even for Γ away from unity. The input polarization is supposed to be homogeneous along the cross-section, and equal to the value taken in $x = 0$. As certified by the dashed-dotted blue lines with triangles in Fig. 6(b), the coupling is improved for each value of $\Gamma \neq 1$, with a very improvement for Γ away from the synchronized case. The coupling efficiency never goes below 90%. When the plane wave solutions from Fig. 2 are used as input conditions, small differences in the polarization are observed: the coupling efficiency is slightly worse (around 10% less) than in the previous case (see Supplement 1), but the beam undergoes a very similar breathing dynamics and the polarization is identical, once the stationary regime is achieved. The possible existence of a quasi-mode subject to lower oscillations remains an open question.

Summarizing our results, we found out that polarization needs to be adjusted in order to achieve a good input coupling away from the resonant case $\Gamma = 1$. Whereas in the monochromatic or quasi-monochromatic regime this implies the introduction of a set of waveplates to adjust the Stokes parameters of the incident field, in the case of ultrashort pulses a strong distortion in the beam spectrum is induced due to the resonant-like response plotted in Fig. 6(b). This point is further stressed out in Fig. 7 where the optical evolution is shown in the two cases discussed above: i) a purely RCP beam with intensity distribution computed for $\Gamma = 1$; ii) an input polarization sharing the same handedness of case (i) but determined by the plane wave model, plus a transverse intensity distributions as provided by Fig. 3. A comparison of the beam cross-sections at $z = 245\ \mu$m in the two cases is provided in Fig. 7(a-f) for six different values of Γ covering all the validity interval of the theory. The coupling is much improved using the

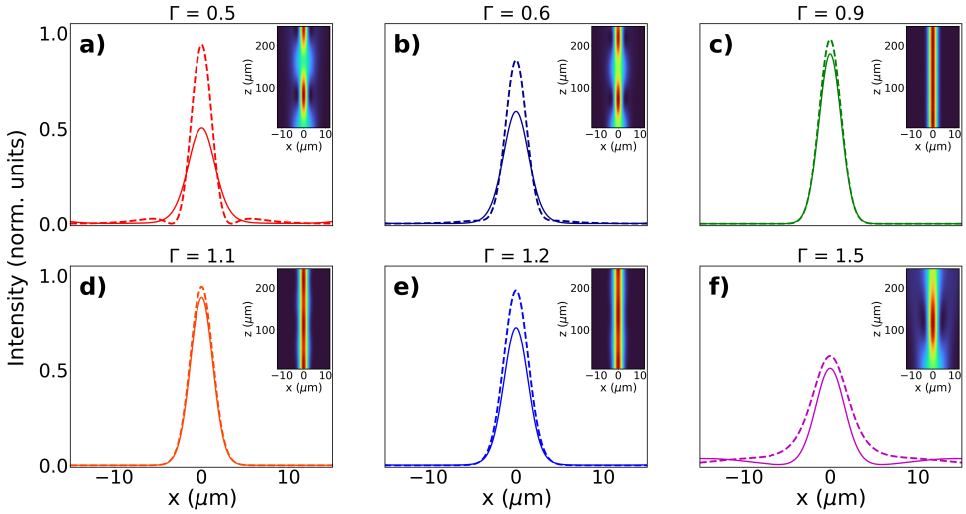

Fig. 7. (a-f) Intensity cross-sections versus x for six different values of Γ (labelled at the top of each pane) at $z = 245\ \mu$m. In all the panels the solid lines correspond to FDTD simulations when the input intensity profile is computed at $\Gamma = 1$ and polarization is right circular; dashed lines is instead the case when the input intensity profile is taken from Fig. 3(b) and the polarization is chosen according to the theoretical predictions. Insets: the corresponding intensity profile on the plane xz when the input polarization is modified according to the theoretical predictions.

Optics EXPRESS

theoretical polarization as input, but the shape of the mode itself does not drastically change. Away from the synchronization (see e.g. $\Gamma = 0.5$ and $\Gamma = 1.5$), side lobes appear in the theoretical case, but they are connected to the breathing the optical beam undergoes, see the insets. As expected, the breathing is minimum near $\Gamma = 1$, where our theory is more accurate. These results suggest that a quasi-mode with a complicated polarization structure exists for any modulation period, but such structured waveform can be found only by using more advanced theories than the simplified model we are using here.

Last, we want to discuss potential experimental realizations of these waveguides. Inscribing an anisotropic structure possessing a point-dependent rotation of the optic axis is challenging, but new technologies capable of achieving this goal emerged in the last few years. Potential candidates are femtosecond-writing of anisotropic structures in glass [28], two-photon polymerization of liquid crystals [29,30], stack of metasurfaces based upon geometric-phase [31,32]. With respect to already established technologies for integrated circuits, a potential venue is to exploit the rotation of the optic axis via the electro-optic effect in thin-film waveguides based upon Lithium Niobate by using patterned electrodes [33].

4. Conclusion

We investigated theoretically and numerically the robustness of the PBP waveguide with respect to deviations from the phase matched condition, that is, when the external modulation is not synchronized with the natural rotation of the polarization. We demonstrated numerically that the mode computed in the synchronized case retains a large degree of confinement (guided power larger than 50%) for wide variations of the external modulations (from 30% to 200%). Theoretically, we modelled the optical propagation exploiting the idea of operator splitting and using the plane wave propagation in longitudinally-modulated anisotropic materials to calculate the phase delay imparted by the inhomogeneous twisting angle. Such a model captures the dependence of the essential ingredients of the waveguiding, such as the Stokes parameters spatial distribution and the size of the guided beam, on the mismatch between the two periods. More importantly, the quasi-modes calculated with our approach are well guided by the twisted anisotropic materials even far away from the phase-matched condition, showing how the PBP waveguides on one side are robust to the geometrical parameters, and on the other side potentially allow the full (polarization and intensity) engineering of the guided mode [34].

Summarizing, our work demonstrates that the optical confinement in the Pancharatnam-Berry waveguides does not depend critically on the period of the modulation, but that a mismatch actually provides an additional degree of freedom in controlling the polarization structuring of the quasi-modes. Our results can be readily extended to the propagation of different wavelengths in a fixed geometry, thus permitting to understand how optical dispersion affects the propagation of ultrashort pulses in this type of electromagnetic waveguides.

Funding. H2020 Marie Skłodowska-Curie Actions (889525); Max Planck School of Photonics; Deutsche Forschungsgemeinschaft (398816777, CRC 1375 NOA).

Acknowledgement. This work used computing resources of the HPC cluster "Draco" at the University of Jena.

Disclosures. The authors declare no conflicts of interest.

Data availability. Data underlying the results presented in this paper are available in Ref. [35].

Supplemental document. See Supplement 1 for supporting content.

References

1. A. Yariv, ed., *Optical Electronics in Modern Communications* (Oxford University, 1997).
2. S. G. Johnson, P. R. Villeneuve, S. Fan, *et al.*, "Linear waveguides in photonic-crystal slabs," Phys. Rev. B **62**(12), 8212–8222 (2000).
3. Q. Lin and S. Fan, "Light guiding by effective gauge field for photons," Phys. Rev. X **4**(3), 031031 (2014).
4. K. Fang and S. Fan, "Controlling the flow of light using the inhomogeneous effective gauge field that emerges from dynamic modulation," Phys. Rev. Lett. **111**(20), 203901 (2013).

Optics EXPRESS

5. A. V. Pankov, I. D. Vatnik, D. V. Churkin, *et al.*, "Observation of localized modes at effective gauge field interface in synthetic mesh lattice," Sci. Rep. **9**(1), 3464 (2019).
6. H. Chalabi, S. Barik, S. Mittal, *et al.*, "Guiding and confining of light in a two-dimensional synthetic space using electric fields," Optica **7**(5), 506–513 (2020).
7. Y. Lumer, M. A. Bandres, M. Heinrich, *et al.*, "Light guiding by artificial gauge fields," Nat. Photonics **13**(5), 339–345 (2019).
8. T. Song, H. Chu, J. Luo, *et al.*, "Ultracompact photonic circuits without cladding layers," Phys. Rev. X **12**(1), 011053 (2022).
9. S. Slussarenko, A. Alberucci, C. P. Jisha, *et al.*, "Guiding light via geometric phases," Nat. Photonics **10**(9), 571–575 (2016).
10. C. P. Jisha, S. Nolte, and A. Alberucci, "Geometric phase in optics: From wavefront manipulation to waveguiding," Laser Photonics Rev. **15**(10), 2100003 (2021).
11. H. Abbaszadeh, M. Fruchart, W. van Saarloos, *et al.*, "Liquid-crystal-based topological photonics," Proc. Natl. Acad. Sci. U. S. A. **118**(4), e2020525118 (2021).
12. M. Berry, "The adiabatic phase and Pancharatnam's phase for polarized light," J. Mod. Opt. **34**(11), 1401–1407 (1987).
13. E. Cohen, H. Larocque, F. Bouchard, *et al.*, "Geometric phase from Aharonov–Bohm to Pancharatnam–Berry and beyond," Nat. Rev. Phys. **1**(7), 437–449 (2019).
14. C. Cisowski, J. B. Götte, and S. Franke-Arnold, "Colloquium: Geometric phases of light: Insights from fiber bundle theory," Rev. Mod. Phys. **94**(3), 031001 (2022).
15. S. Pancharatnam, "Generalized theory of interference, and its applications," Proc. - Indian Acad. Sci., Sect. A **44**(5), 247–262 (1956).
16. R. Bhandari, "Polarization of light and topological phases," Phys. Rep. **281**(1), 1–64 (1997).
17. Z. Bomzon, G. Biener, V. Kleiner, *et al.*, "Space-variant Pancharatnam–Berry phase optical elements with computer-generated subwavelength gratings," Opt. Lett. **27**(13), 1141–1143 (2002).
18. C. P. Jisha, A. Alberucci, L. Marrucci, *et al.*, "Interplay between diffraction and the Pancharatnam-Berry phase in inhomogeneously twisted anisotropic media," Phys. Rev. A **95**(2), 023823 (2017).
19. D. S. Hum and M. M. Fejer, "Quasi-phasematching," C. R. Physique **8**(2), 180–198 (2007).
20. C. P. Jisha, A. Alberucci, J. Beeckman, *et al.*, "Self-trapping of light using the Pancharatnam–Berry phase," Phys. Rev. X **9**(2), 021051 (2019).
21. M. V. Berry, "Pancharatnam, virtuoso of the Poincaré sphere: an appreciation," Curr. Sci. **67**, 220–223 (1994).
22. R. C. Jones, "A new calculus for the treatment of optical systemsi. description and discussion of the calculus," J. Opt. Soc. Am. **31**(7), 488–493 (1941).
23. J. D. Hunter, "Matplotlib: A 2d graphics environment," Comput. Sci. Eng. **9**(3), 90–95 (2007).
24. C. R. Harris, K. J. Millman, S. J. van der Walt, *et al.*, "Array programming with NumPy," Nature **585**(7825), 357–362 (2020).
25. J. C. Gutiérrez-Vega, "Pancharatnam–Berry phase of optical systems," Opt. Lett. **36**(7), 1143–1145 (2011).
26. A. F. Oskooi, D. Roundy, M. Ibanescu, *et al.*, "MEEP: A flexible free-software package for electromagnetic simulations by the FDTD method," Comput. Phys. Commun. **181**(3), 687–702 (2010).
27. C. P. Jisha, S. V. Arumugam, L. Marrucci, *et al.*, "Waveguiding driven by the Pancharatnam-Berry phase," Phys. Rev. A **107**(1), 013523 (2023).
28. M. Sakakura, Y. Lei, L. Wang, *et al.*, "Ultralow-loss geometric phase and polarization shaping by ultrafast laser writing in silica glass," Light: Sci. Appl. **9**(1), 15 (2020).
29. C. C. Tartan, P. S. Salter, T. D. Wilkinson, *et al.*, "Generation of 3-dimensional polymer structures in liquid crystalline devices using direct laser writing," RSC Adv. **7**(1), 507–511 (2017).
30. Z. He, G. Tan, D. Chanda, *et al.*, "Novel liquid crystal photonic devices enabled by two-photon polymerization," Opt. Express **27**(8), 11472–11491 (2019).
31. Y. Zhou, I. I. Kravchenko, H. Wang, *et al.*, "Multilayer noninteracting dielectric metasurfaces for multiwavelength metaoptics," Nano Lett. **18**(12), 7529–7537 (2018).
32. M. Kim, N.-R. Park, A. Yu, *et al.*, "Multilayer all-polymer metasurface stacked on optical fiber via sequential micro-punching process," Nanophotonics **12**(13), 2359–2369 (2023).
33. D. Zhu, L. Shao, M. Yu, *et al.*, "Integrated photonics on thin-film lithium niobate," Adv. Opt. Photonics **13**(2), 242–352 (2021).
34. S. Kiriushechkina, A. Vakulenko, D. Smirnova, *et al.*, "Spin-dependent properties of optical modes guided by adiabatic trapping potentials in photonic Dirac metasurfaces," Nat. Nanotechnol. **18**(8), 875–881 (2023).
35. S. V. Arumugam, C. P. Jisha, L. Marrucci, *et al.*, "Dataset for the paper "Exploring the Impact of Longitudinal Modulation on the Twisting Angle in Pancharatnam-Berry Phase-Based Waveguides"," Zenodosus (2023). https://doi.org/10.5281/zenodo.10069332.